

Thermal diode with switchable cloaking effect enabled by asymmetric temperature-dependent thermal conductivity

Mengzhen Xue(薛梦贞), Jun Wang(王军), and Guodong Xia(夏国栋)
Citation: Chin. Phys. B, 2025, 34 (**11**): 114403. DOI: 10.1088/1674-1056/ae118b
http://cpb.iphy.ac.cn; http://iopscience.iop.org/cpb

What follows is a list of articles you may be interested in

Giant thermal rectification beyond structural asymmetry via current-induced nonreciprocity effects

Jiayao Zhang(张佳瑶), Yu Hao(郝雨), Bowen Xiong(熊博文), Shanhe Su(苏山河), and Zhimin Yang(杨智敏)
Chin. Phys. B, 2025, 34 (**9**): 094402. DOI: 10.1088/1674-1056/add906

Enhancement of thermal rectification by asymmetry engineering of thermal conductivity and geometric structure for multi-segment thermal rectifier

Fu-Ye Du(杜甫烨), Wang Zhang(张望), Hui-Qiong Wang(王惠琼), and Jin-Cheng Zheng(郑金成)
Chin. Phys. B, 2023, 32 (**6**): 064402. DOI: 10.1088/1674-1056/acc78c

Thermal rectification induced by Wenzel-Cassie wetting state transition on nano-structured solid-liquid interfaces

Haiyang Li(李海洋), Jun Wang(王军), and Guodong Xia(夏国栋)
Chin. Phys. B, 2023, 32 (**5**): 054401. DOI: 10.1088/1674-1056/aca9c1

A phononic rectifier based on carbon schwarzite host-guest system

Zhongwei Zhang(张忠卫), Yulou Ouyang(欧阳宇楼), Jie Chen(陈杰), and Sebastian Volz
Chin. Phys. B, 2020, 29 (**12**): 124402. DOI: 10.1088/1674-1056/abbbf9

General theories and features of interfacial thermal transport

Hangbo Zhou(周杭波), Gang Zhang(张刚)
Chin. Phys. B, 2018, 27 (**3**): 034401. DOI: 10.1088/1674-1056/27/3/034401

SPECIAL TOPIC — Heat conduction and its related interdisciplinary areas

Thermal diode with switchable cloaking effect enabled by asymmetric temperature-dependent thermal conductivity

Mengzhen Xue(薛梦贞), Jun Wang(王军)†, and Guodong Xia(夏国栋)

Beijing Key Laboratory of Heat Transfer and Energy Conversion, Beijing University of Technology, Beijing 100124, *China*

(Received 13 June 2025; revised manuscript received 16 September 2025; accepted manuscript online 10 October 2025)

Thermal rectification refers to the asymmetry in heat transfer capability when subjected to forward and reverse temperature gradients. A thermal cloak can render objects invisible in thermal fields by redirecting heat flux pathways. In this paper, we present a thermal diode model based on a bi-layer thermal cloak system that incorporates a composite heat-flux-attracting layer with asymmetric, temperature-dependent thermal conductivity. In the forward case, the heat flux bypasses the cloaking region while maintaining undistorted background isotherm contours, whereas in the reverse case, the thermal cloak fails to function and the device effectively insulates heat. Consequently, thermal rectification occurs in the bi-layer thermal cloak system. A significant increase in the thermal rectification ratio is observed as the temperature gradient increases. By optimizing the system dimensions, a peak rectification ratio of 11.06 is achieved. This study provides physical insight and a design framework for developing novel thermal diodes with dual-functional thermal management capabilities.

Keywords: thermal rectification, thermal cloak, temperature-dependent thermal conductivity, bulk material

PACS: 44.10.+i, 05.60.–k, 81.05.Zx

DOI: 10.1088/1674-1056/ae118b **CSTR:** 32038.14.CPB.ae118b

1. Introduction

The thermal rectification effect refers to the phenomenon of asymmetric heat transfer under forward versus reverse temperature gradients; namely, the magnitude of the heat flux depends on the direction of the applied thermal bias.[1–5] In a thermal diode, the heat flux is significantly larger in one direction than in the opposite direction. This phenomenon has potential applications in many fields, including waste heat recovery,[6,7] thermal management of electronic devices,[8,9] quantum information systems,[10,11] room-temperature magnetocaloric applications,[12] and flexible wearable thermal management,[13] and has therefore attracted broad attention.

Thermal diodes serve as essential devices for regulating and directing the flow of heat. Terraneo *et al.*[3] proposed the concept of a thermal diode in a three-segment nonlinear lattice model, wherein the underlying physical mechanism relies on a temperature-dependent power spectrum. In 2004, Li *et al.*[4] proposed a two-segment thermal diode model with Frenkel–Kontorova chains, in which the rectification ratio can be increased by two orders of magnitude owing to phonon spectrum mismatch at the interface. Later, in their subsequent study, an additional order of magnitude improvement in the rectification effect was achieved.[5] Chang *et al.*[14] experimentally demonstrated the thermal rectification effect in mass-loaded nanotubes, with asymmetrically deposited boron nitride nanotubes (BNNTs) exhibiting the most pronounced thermal diode behavior. For nanostructures, the phonon scattering and the efficiency of thermal rectification can be influenced by temperature, geometry,[15,16] interface structure,[16–19] and quantum coherence.[20] On the other hand, for bulk materials, the temperature dependence of thermal conductivity has been identified as another key mechanism behind thermal rectification. For example, thermal rectification can be achieved by selecting materials at both ends with opposite temperature dependencies of thermal conductivity.[21] This design, which relies on the temperature-dependent thermal conductivity of materials to regulate the direction of heat flow, has also been discussed from a theoretical perspective,[22] and extended to macroscopic applications through numerical simulations and material performance estimations.[23] Subsequent studies further achieved quantitative modeling and experimental verification.[24] It was revealed that the essential condition for achieving thermal rectification in bulk materials lies in the thermal conductivity being a function of both space and temperature, which can be realized through either composite structures or properly engineered monolithic materials.[25] In addition, introducing zigzag interfaces[26] or multi-segment geometric gradients[27] can regulate the temperature sensitivity and spatial distribution of thermal conductivity, further enhancing the rectification effect. Li *et al.*[28] also discussed the effectiveness of several typical mechanisms for realizing diffusion nonreciprocity and fabricating thermal diodes, demonstrating the equivalence between breaking steady-state global reciprocity and achieving a thermal diode. This provided an

†Corresponding author. E-mail: jwang@bjut.edu.cn

© 2025 Chinese Physical Society and IOP Publishing Ltd. All rights, including for text and data mining, AI training, and similar technologies, are reserved.

important theoretical basis for the realization of macroscopic thermal diodes.

The temperature-dependent nature of thermal conductivity provides a fundamental theoretical framework for understanding thermal rectification and for constructing temperature-dependent thermal cloaking devices.[29–31] The concept of a thermal cloak was introduced by Fan *et al.*[32] based on a first-principles approach that established a theory of steady-state transformation thermotics. To avoid the complex calculations involved in transformation thermotics, Han *et al.*[33] proposed a two-layer thermal cloak structure. Based on this bi-layer cloak, a thermal camouflage device was designed to transform the thermal scattering signature of an object into that of multiple expected targets, achieving both cloaking and camouflage effects in heat conduction.[34] The methods based on transformation thermotics[35–39] and bulk materials[40–44] represent two key strategies for achieving the thermal cloaking effect. However, since the thermal conductivity of most materials in nature varies with temperature, it is necessary to consider temperature dependence when studying thermal cloaks. Li *et al.*[29,30] combined temperature-dependent thermal conductivity with transformation thermotics to design tunable thermal invisibility materials, enabling dynamic switching of heat flux paths, and further extended this approach to the design of macroscopic thermal diodes. To address the complexity of transformation thermotics and the challenges of material fabrication, Xue *et al.*[31] proposed a switchable thermal cloaking effect using a bi-layer thermal cloak based on temperature-dependent thermal conductivity, which exhibits rapid switching of invisibility performance near the critical temperature.

It has been demonstrated that non-uniform media can exhibit quasi-uniform heat conduction through effective medium theory with periodicity. This property enables the design of novel periodic composites for thermal camouflage and rectification. In particular, the concepts of "Janus thermal illusion" and "illusion thermal diodes" demonstrate the ability to achieve invisibility and visibility illusions simultaneously through periodic structures.[45] However, most existing research still focuses on either thermal rectification or thermal cloaking, with limited exploration of their combination. The concept of temperature-dependent transformation thermotics proposed in Ref. [29] enables switchable thermal cloaks and macroscopic thermal diodes. In this method, anisotropic and spatially varying thermal conductivity tensors are obtained from a coordinate transformation dependent on temperature. Practical realization requires either anisotropic effective media or structural deformation, which presents significant fabrication challenges. Considering the need for macroscopic heat flux regulation in practical devices, exploring thermal rectification mechanisms in bulk materials remains a core challenge of current research.

In this paper, we propose a bi-layer structure composed of isotropic bulk materials, featuring a composite heat-flux-attracting layer to achieve synergistic regulation of thermal rectification and cloaking effects. The composite heat-flux-attracting layer is constructed from materials A and B, which possess asymmetric temperature-dependent thermal conductivities. Numerical simulations are conducted to analyze how thermal conductivity and system size affect the thermal rectification ratio. This approach greatly simplifies the design and enables straightforward parameter optimization. The findings offer a novel strategy for designing thermal diodes that achieve both efficient rectification and cloaking effects. The proposed method is applicable to fields such as aerospace and microelectronics that require precise heat flow control and thermal protection,[46] and provides innovative approaches for active control of heat flow direction and pathways.

2. System design

2.1. Thermal rectifier model with composite heat-flux-attracting layer

In a bi-layer thermal cloak model, an inner insulation layer is used to repel the heat flux, while an outer layer with higher thermal conductivity (the heat-flux-attracting layer) is used to attract the heat flux repelled by the inner layer. As shown in Fig. 1(a), the red region represents the cloaking area ($r < r_c$), with a thermal conductivity of $k_0 = 10$ W·m^{-1}·K^{-1}. The gray region corresponds to the inner layer ($r_c < r < r_i$), which has a very low thermal conductivity of $k_1 = 0.03$ W·m^{-1}·K^{-1}, acting as an adiabatic layer. The green region represents the outer layer ($r_i < r < r_u$) with higher thermal conductivity k_2, serving as the heat-flux-attracting layer that also eliminates the distortion of the temperature distribution caused by the presence of internal objects. The blue region denotes the surrounding area with thermal conductivity $k_3 = 2.3$ W·m^{-1}·K^{-1}.

For a two-dimensional thermal cloak, when the inner layer is a perfect adiabatic material ($k_1 = 0$ W·m^{-1}·K^{-1}), the thermal conductivity of the outer layer is given by[33]

$$k_2 = \frac{r_u^2 + r_i^2}{r_u^2 - r_i^2} k_3. \tag{1}$$

In this study, the model dimensions are consistent with those used in Ref. [33], specifically $r_c = 6$ mm, $r_i = 9.5$ mm, and $r_u = 12$ mm. The surrounding region size is set to 30 mm × w, where w represents the width of the system, with $w = r_u = 12$ mm in this case. For $k_3 = 2.3$ W·m^{-1}·K^{-1}, the thermal conductivity of the outermost layer (heat-flux-attracting layer) material should be $k_2 \approx 10$ W·m^{-1}·K^{-1} to guarantee a perfect cloaking effect. Following the theoretical

framework in Ref. [33], the central region ($r < r_c$) in this design serves as the cloaked object, and its material properties do not affect the external temperature distribution.

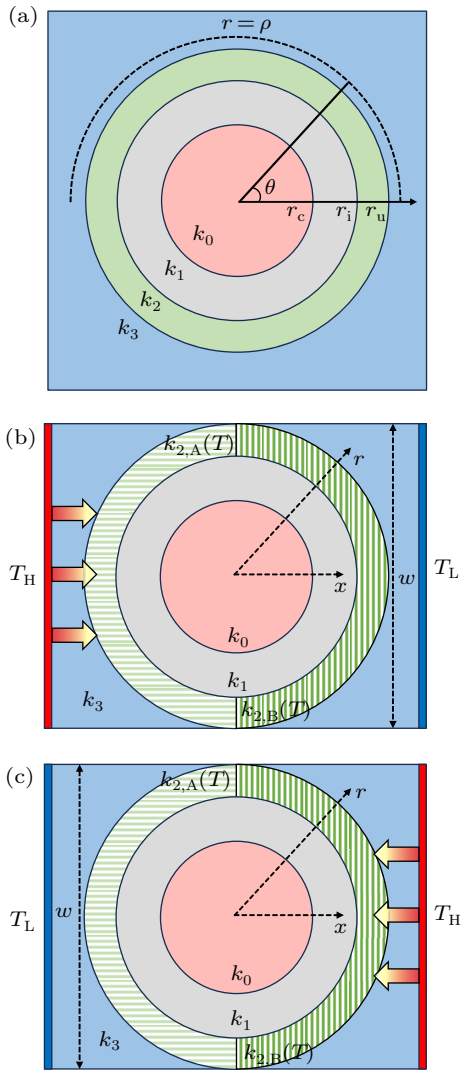


Fig. 1. (a) Cross-sectional view of the bi-layer thermal cloak; (b) and (c) schematic diagrams of a thermal rectification system with a composite heat-flux-attracting layer: (b) forward-bias mode; (c) reverse-bias mode.

Figure 2 illustrates the variation of the temperature gradient at $r = \rho$ for different thermal conductivities of the inner layer. When the temperature difference is 120 K, the temperature gradient along the selected dashed line $r = \rho$ in Fig. 1(a) reaches approximately 4000 K·m^{-1}. It can be seen that the temperature gradient approaches the ideal criterion for a perfect cloak when $k_1 = 0.003$ W·m^{-1}·K^{-1} (approaching a perfectly adiabatic condition), and the cloaking performance of the bi-layer thermal cloak is correspondingly enhanced. As k_1 increases (0.05 W·m^{-1}·K^{-1}, 0.1 W·m^{-1}·K^{-1}, 0.3 W·m^{-1}·K^{-1}), the temperature gradient gradually deviates from 4000 K·m^{-1} at $r = \rho$, indicating a weakened cloaking effect.

Nevertheless, for $k_1 = 0.03$ W·m^{-1}·K^{-1}, the temperature gradient profile differs very little from that for $k_1 = 0.003$ W·m^{-1}·K^{-1}. Therefore, it can be assumed that the inner material with this thermal conductivity exhibits excellent thermal insulation performance and can act as an adiabatic layer, thereby satisfying the condition under which Eq. (1) is valid.

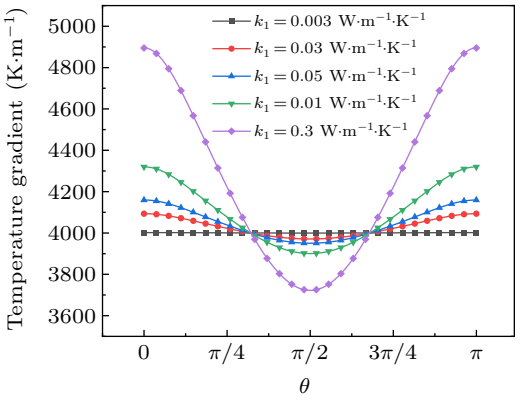


Fig. 2. Temperature gradient at $r = \rho$ in a bi-layer thermal cloak for varying inner-layer thermal conductivity k_1.

Various models have been proposed to describe temperature-dependent thermal conductivity, such as the linear models $k(T) = mT + c$,[47] $k(T) = k_0(1 + \alpha T)$,[48] and the power-law model $k(T) = k_0(T/T_0)^{\alpha}$.[24] For certain materials, particularly phase-change materials, the variation of thermal conductivity with temperature generally follows a sigmoidal curve.[49] The thermal conductivity of such materials shows a rapid transition near a specific temperature and eventually saturates as the temperature further changes. This feature enables them to automatically adjust their thermal conductivity in response to the actual temperature environment, thereby better satisfying the complex requirements of thermal design. Motivated by this property, the Sigmoidal function is adopted in this work to characterize the material's temperature-dependent thermal conductivity.

Since the inner layer of the system is designed to possess extremely low thermal conductivity, it effectively protects the cloaking region from external heat flux. Therefore, the temperature dependence of the inner-layer thermal conductivity k_1 is negligible in the present model.

We propose a thermal rectification model with a composite outer layer composed of two different materials, as illustrated in Figs. 1(b) and 1(c). The temperature-dependent thermal conductivity of material A ($k_{2,A}$) on the left side of the composite heat-flux-attracting layer increases with temperature, while that of material B ($k_{2,B}$) on the right side decreases. Their temperature-dependent thermal conductivities are assumed to be

$$k_{2,A}(T) = k_H + \frac{k_L - k_H}{1 + \exp(\beta(T - T_{ref}))}, \tag{2}$$

$$k_{2,B}(T) = k_L - \frac{k_L - k_H}{1 + \exp(\beta(T - T_{ref}))]}. \tag{3}$$

Here, $(1+\exp(-x))^{-1}$ is a typical sigmoidal function that produces a rapid transition from k_{L} to k_{H} around the reference temperature T_{ref}. The parameter β controls the sharpness of this transition. These mirrored thermal conductivity functions describe asymmetric thermal responses, enabling thermal rectification.[30] Although the functional form is somewhat idealized, the underlying physical mechanism is achievable in practice.[49–51] For example, certain phase-change materials such as VO_2 exhibit a sharp increase in thermal conductivity near their phase transition temperature,[49] while polyethylene nanofibers display a gradual decrease with increasing temperature,[51] forming an opposite "on/off" behavior. Moreover, the critical transition temperature or switching range can be tuned via doping, thickness modulation, or nanoscale structural design.[50,51]

Under the forward thermal bias (Fig. 1(a)), the system has a hot side T_{H} on the left and a cold side T_{L} on the right, and the total heat current density j_{F} flows from material A to B. In the reverse case (Fig. 1(b)), the hot and cold sides are swapped, and the heat current density j_{R} reverses direction. According to Eqs. (2) and (3), in the forward case, both materials exhibit higher thermal conductivity, whereas in the reverse case, they show lower values. Thus, asymmetric heat transfer occurs ($j_{\mathrm{F}} > j_{\mathrm{R}}$), demonstrating thermal rectification. The thermal rectification ratio γ is defined as

$$\gamma = \left|\frac{j_{\mathrm{F}}}{j_{\mathrm{R}}}\right| - 1. \tag{4}$$

When j_{F} and j_{R} are equal, there is no thermal rectification ($\gamma = 0$), while larger γ indicates stronger rectification.

3. Analysis of thermal rectification and cloaking characteristics

Numerical simulations are conducted using COMSOL Multiphysics, and a computational model, as shown in Fig. 1(a), is established. According to Eq. (1), the required thermal conductivity of the outer layer for the thermal cloak to operate is approximately 10 $\mathrm{W{\cdot}m^{-1}{\cdot}K^{-1}}$. Thus, the upper limit of the thermal conductivity of the composite heat-flux-attracting layer is therefore selected as $k_{\mathrm{H}} = 9.8$ $\mathrm{W{\cdot}m^{-1}{\cdot}K^{-1}}$. The lower limit is the same as that of the adiabatic layer, i.e., $k_{\mathrm{L}} = 0.03$ $\mathrm{W{\cdot}m^{-1}{\cdot}K^{-1}}$. The reference temperature is set to $T_{\mathrm{ref}} = 343$ K, and the scaling factor is $\beta = 0.2$ $\mathrm{K^{-1}}$.

Material A on the left approaches k_{H} when the temperature exceeds T_{ref}, whereas material B on the right reaches k_{H} when the temperature is much lower than T_{ref}.

The heat current density j is obtained by integrating the x-component of the heat flux along the line $x = 0$. The heat flux represents the rate of heat transfer per unit area, indicating the local intensity of heat flow at a given position. Specifically, the heat current density j denotes the net heat transferred per unit width across this region, calculated by integrating the local heat flux.

The dimensionless temperature difference Δ is defined as

$$\Delta = \frac{T_{\mathrm{H}} - T_{\mathrm{L}}}{T_{\mathrm{ref}}},$$

and the reference temperature

$$T_{\mathrm{ref}} = \frac{T_{\mathrm{H}} + T_{\mathrm{L}}}{2}$$

is chosen as the switching point for the temperature-dependent thermal conductivity functions, ensuring opposite thermal states on the two sides of the system.

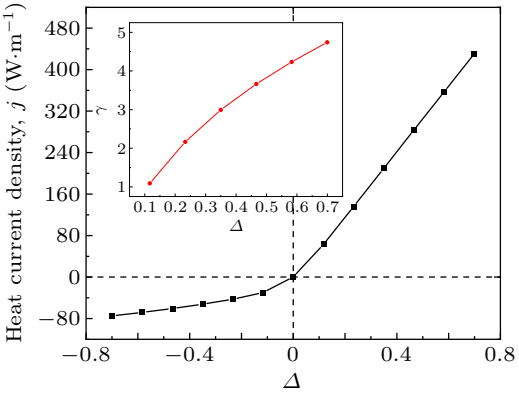


Fig. 3. Heat current density and thermal rectification ratio versus the dimensionless temperature difference. The total heat current density j is calculated by integrating the x-component of the heat flux along $x = 0$.

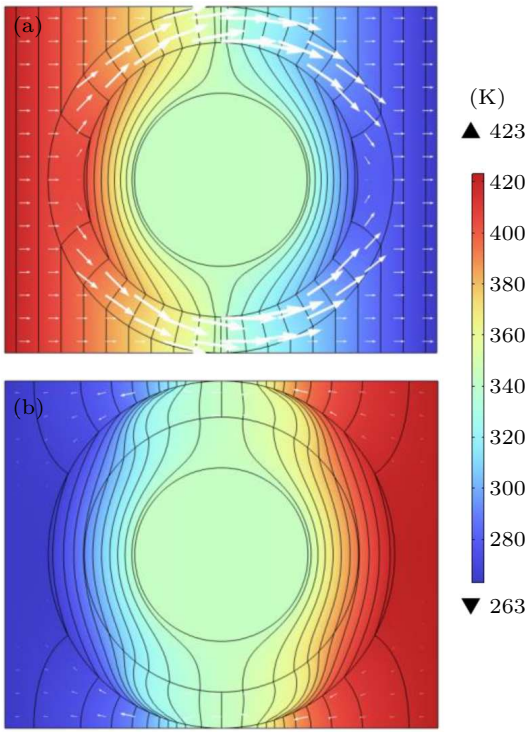


Fig. 4. Thermal rectifier obtained from two-dimensional finite-element simulations. The black lines represent isotherms, and the white arrows indicate the direction of heat flux. The arrow lengths correspond to the magnitude of the heat flux: (a) forward case with cloaking effect; (b) reverse case without cloaking effect.

Figure 3 presents the total heat current density (j) and thermal rectification ratio of the thermal rectifier under various dimensionless temperature differences Δ in both the forward and reverse cases. As expected, j in the forward case is significantly higher than that in the reverse case. Moreover, this discrepancy increases with Δ, leading to a gradual increase in the thermal rectification ratio. Figure 4 illustrates the thermal rectification and cloaking effects of the rectifier in both cases for $T_{\mathrm{H}} = 423$ K and $T_{\mathrm{L}} = 263$ K. As shown in Fig. 4(a), the heat flux can easily bypass the intermediate region and restore the isothermal distribution distorted by the internal object, indicating that the thermal cloak works quite well in the forward case. However, in the reverse direction, the cloak fails to function effectively, and the device acts as a thermal insulator. Therefore, owing to the asymmetry of the composite heat-flux-attracting layer, thermal rectification is achieved in this bi-layer thermal cloak model.

4. Analysis of thermal rectification effect

4.1. Impact of thermal conductivity bounds on rectification efficiency

In Fig. 3, with $k_{\mathrm{H}} = 9.8$ W·m^{-1}·K^{-1} and $k_{\mathrm{L}} = 0.03$ W·m^{-1}·K^{-1}, the rectification ratio increases from $\gamma = 1.09$ to 4.74 as the dimensionless temperature difference increases. However, the temperature-dependent thermal conductivity of the outermost layer spans a wide range (nearly three orders of magnitude). Considering that the thermal conductivity of common materials usually does not vary so dramatically, six specific cases of the thermal conductivity bounds are considered in this paper and defined as Case-I to Case-VI, with detailed parameters provided in Table 1. This categorization enables a more detailed analysis of the specific influence of thermal conductivity on rectification performance.

Table 1. Thermal conductivity bounds.

Case	I	II	III	IV	V	VI
k_{L} (W·m^{-1}·K^{-1})	0.03	0.1	0.15	0.03	0.1	0.15
k_{H} (W·m^{-1}·K^{-1})	9.8	9.8	9.8	6	6	6

Figure 5(a) shows the variation of the total heat current density with temperature. It can be seen that in Case-IV, V, and VI (with an upper thermal conductivity bound of 6 W·m^{-1}·K^{-1}), the heat current densities under forward thermal bias are generally lower than those in Case-I, I, and III (with an upper limit of 9.8 W·m^{-1}·K^{-1}). This is because, in the forward case, both materials A and B reach their upper thermal conductivity bounds. According to Fourier's law ($j = -k_2(T) \cdot (\mathrm{d}T/\mathrm{d}x)$), the heat current density in Case-I, II, and III ($k_{\mathrm{H}} = 9.8$ W·m^{-1}·K^{-1}) is higher than that in Case-IV, V, and VI ($k_{\mathrm{H}} = 6$ W·m^{-1}·K^{-1}). As shown in Fig. 5(b), the difference in heat current density between the forward and reverse modes increases with the temperature difference, leading to a higher rectification ratio. When $\Delta = 0.7$, the thermal rectification ratio decreases from $\gamma = 4.74$ to 3.29, which is still a considerable improvement. Even though the thermal conductivity range is narrowed, the rectification ratio remains at an acceptable level.

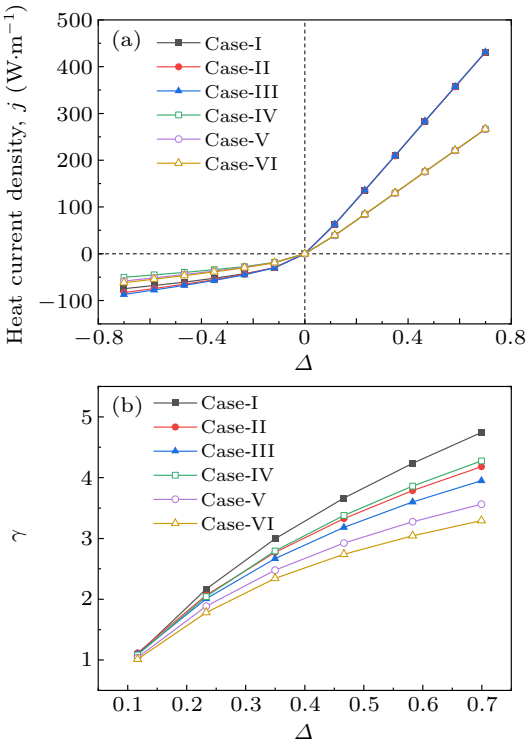


Fig. 5. (a) Variation of heat current density with dimensionless temperature difference. (b) Variation of thermal rectification ratio with dimensionless temperature difference for various cases.

4.2. Influence of system sizes on rectification efficiency

In the aforementioned simulations, the rectification ratio can reach 4.74, which is moderate. Even though the bi-layer thermal cloak is switched off in the reverse case, the lower limit of the composite heat-flux-attracting layer's thermal conductivity is higher than the ideal value, resulting in insufficient system adiabaticity. Consequently, the relatively high reverse heat current density limits the rectification effect. By reducing the width of the model (w), the system approaches an adiabatic condition, so that the reverse heat current density j_{R} can be suppressed, thereby enhancing the thermal rectification effect.

As shown in Fig. 6, the composite heat-flux-attracting layer of the thermal rectifier in Fig. 1 is truncated to explore the effect of system width on the thermal rectification ratio by varying w. To ensure the thermal cloaking performance of the system, w should not be less than the diameter of the adiabatic layer (19 mm). Good contact between the materials and the heat sources is assumed. In this two-dimensional conduction thermal model, the total heat current density through the thermal rectifier is obtained by integrating Fourier's law.

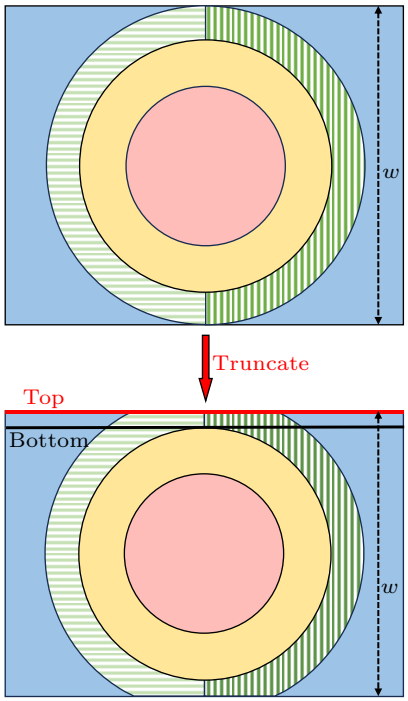


Fig. 6. Variation of the thermal rectifier size w. The red and black lines denote the top and bottom boundaries of the composite heat-flux-attracting layer, respectively.

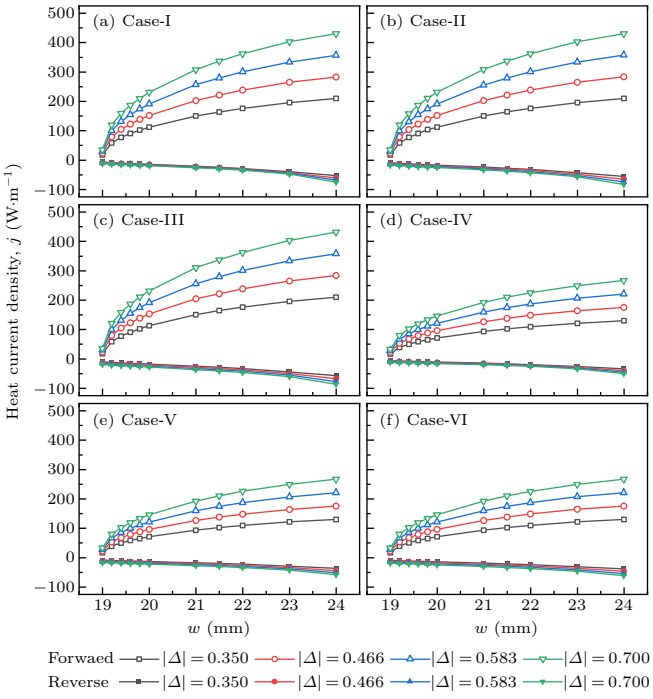


Fig. 7. Heat current density versus the system size w under different temperature differences for (a) Case-I, (b) Case-II, (c) Case-III, (d) Case-IV, (e) Case-V, and (f) Case-VI.

Figure 7 illustrates the relationship between the heat current density and system size. The dimensionless temperature differences are set at $\Delta = 0.350$, 0.466, 0.583, and 0.700. For $w = 19$ mm, the thermal cloak is in the off state, and the heat current densities for the forward and reverse cases are close to each other. When w is slightly larger than 19 mm, the thermal cloak rapidly transitions from the off to the on state. This results in a rapid increase of the forward heat current density, giving rise to the rectification effect. The heat current density through the rectifier increases with system size for both forward and reverse cases.

The magnitude of the rectification ratio depends on the ratio of the forward to reverse heat current densities. Figure 8 shows the relationship between the thermal rectification ratio γ and the system size w. For all six cases, γ rises rapidly to a maximum and then decreases slowly as w increases from 19 mm to 24 mm. Case-I and Case-VI exhibit the largest and smallest variations in rectification ratio, respectively. For Case-I, the rectification ratio γ rises from 1.95 to 11.06 due to the sharp increase of the forward heat current density at $\Delta = 0.700$; subsequently, γ gradually decreases to 4.74 as the reverse heat current density increases. In contrast, Case-VI demonstrates a more moderate trend. At $\Delta = 0.350$, γ rises sharply from 0.73 to 3.83 and then gradually decreases to 2.74. Therefore, the rectification ratio exhibits significant dependence on system size at different temperature differences. Even for smaller temperature differences and narrower thermal conductivity bounds, the rectification ratio can be significantly enhanced by adjusting the system size.

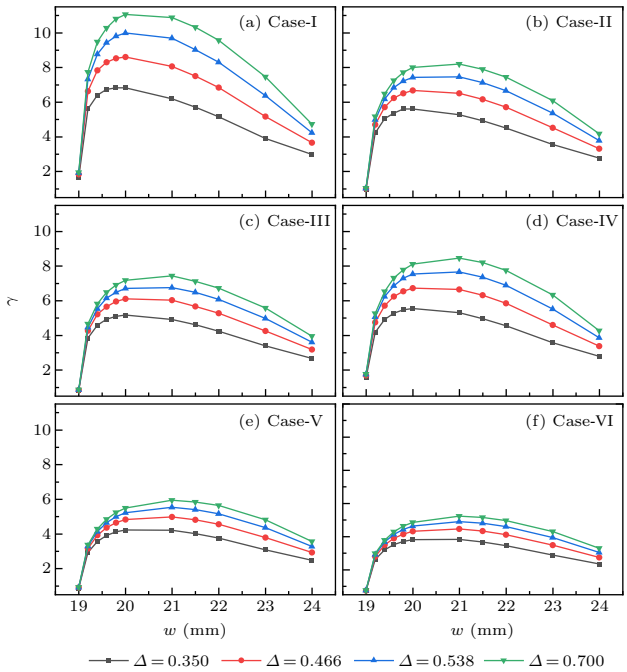


Fig. 8. Thermal rectification ratio versus the system size w under different temperature differences for (a) Case-I, (b) Case-II, (c) Case-III, (d) Case-IV, (e) Case-V, and (f) Case-VI.

Figures 9 and 10 respectively present the temperature distribution and local heat flux distribution of the thermal rectifier for $w = 19$ mm, 19.2 mm, 19.4 mm, 20 mm, 22 mm, and 24 mm. For $w = 19$ mm, the external composite heat-flux-attracting layer is completely truncated in the vertical direction. In the forward case, the heat flux cannot effectively

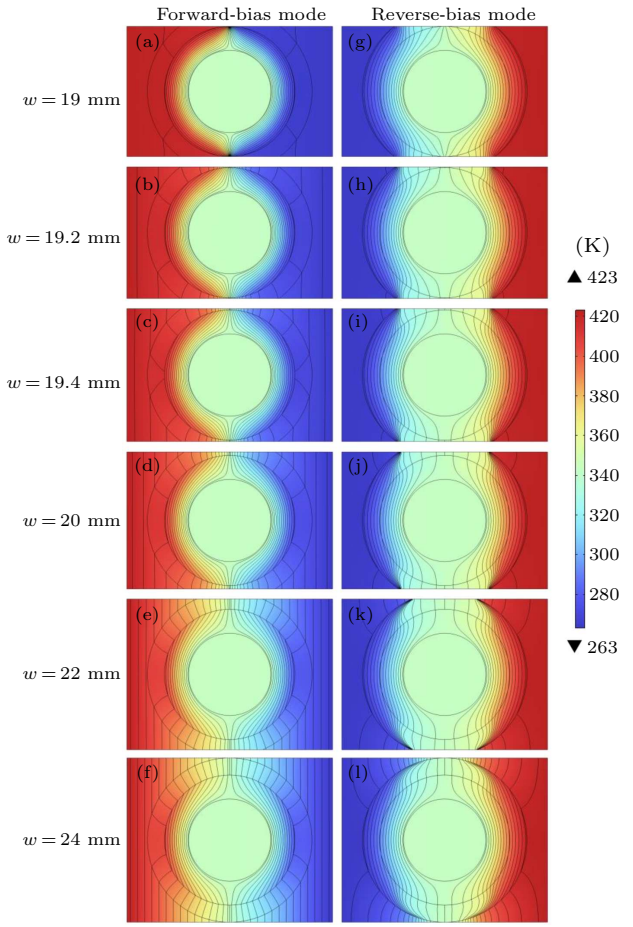


Fig. 9. Temperature distribution for different system sizes: (a)–(f) for the rectifier under forward thermal bias and (g)–(l) under reverse thermal bias. Black lines represent isotherms. Parameters are set as Case-I, $\Delta = 0.466$.

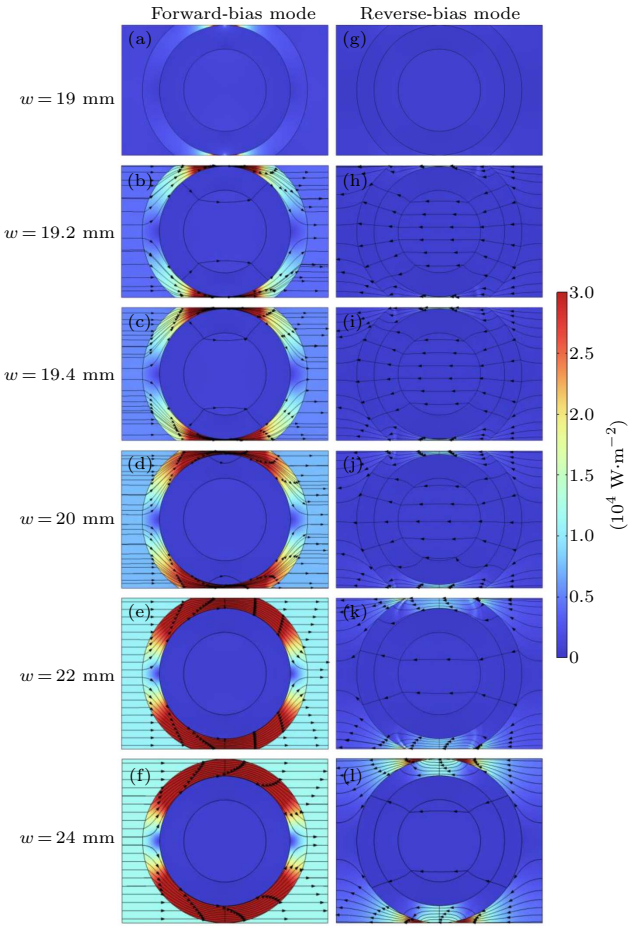


Fig. 10. Heat flux distribution for different system sizes: (a)–(f) for the rectifier under forward thermal bias and (g)–(l) under reverse thermal bias. Black arrows indicate the direction of heat flux. Parameters are set as Case-I, $\Delta = 0.466$.

bypass the outer layer, resulting in nearly zero heat flux for both directions and, consequently, a negligible rectification effect. As w increases, the forward heat current density (j_F) rises rapidly because heat fluxes can bypass the insulating layer along the outer layer. In the reverse case, the low thermal conductivity of the outer layer causes the thermal cloak to lose its cloaking effect. The heat flux converges at the interface between the peripheral region and the outer layer and crosses into the left material A, following the path of least thermal resistance. This asymmetry in heat flux magnitude leads to a substantial increase in the rectification ratio.

Since the thermal conductivity of the inner layer is very low, the heat flux mainly flows through the composite heat-flux-attracting layer of the outer layer. Figure 11 shows the local thermal resistance distribution of the composite heat-flux-attracting layer for different system sizes. In the two-dimensional finite element model, to define thermal resistance meaningfully, we assume that δ is the thickness perpendicular to the paper surface. The local thermal resistance R_{th} is then defined as $R_{\mathrm{th}}(x) = \Delta T(x)/(j(x)\cdot\delta)$, where $\Delta T(x)$ is the local temperature difference between the high-temperature heat source and the edge of the composite heat-flux-attracting layer

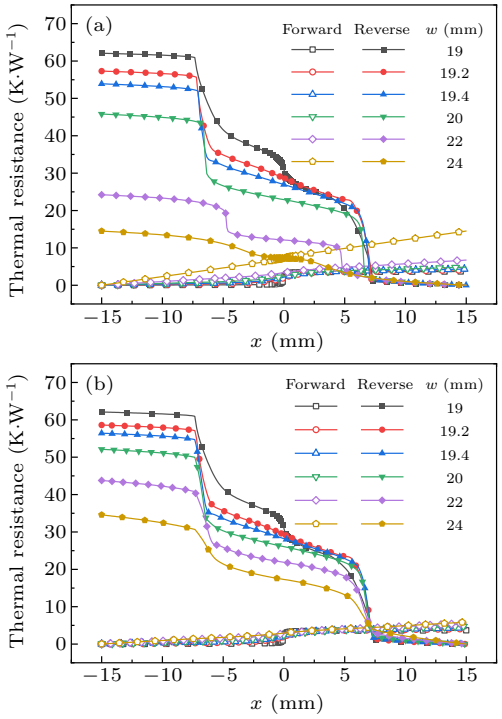


Fig. 11. Thermal resistance versus position for forward and reverse modes: (a) top boundary of the composite heat-flux-attracting layer, (b) bottom boundary of the composite heat-flux-attracting layer. The layer thickness is $\delta = 30$ mm.

at position x, and $j(x)$ (W·m^{-1}) is the heat current density per unit thickness along the x direction. The product $j(x)\cdot\delta$ gives the actual heat flow (W) at that position. At the top and bottom of the outer layer (see Fig. 6 for reference), the thermal resistance in the forward case is always lower than in the reverse case. This indicates that the forward heat current density ($j_{\rm F}$) is higher than the reverse counterpart ($j_{\rm R}$), yielding a high rectification ratio. However, as w increases, the heat flux channel broadens, resulting in a rapid decrease in reverse thermal resistance at the top and bottom. This allows reverse heat flux to enter more easily from the interface between the peripheral region and the outer layer, enhancing the reverse heat current density. Therefore, increasing the system size can significantly reduce the thermal resistance in the reverse case while minimally affecting the forward resistance, which causes the thermal rectification effect to decrease at larger w.

5. Conclusion

In summary, the synergistic design of thermal rectification and thermal cloaking is successfully realized through a composite heat-flux-attracting layer with temperature-dependent thermal conductivities. Numerical results indicate that, in the forward case, the high thermal conductivity enables efficient heat transfer and preserves the thermal cloaking effect without distorting the surrounding isotherms. In the reverse case, the reduced thermal conductivity hinders heat flux and leads to cloaking failure. Even when the thermal conductivity variation is limited to a finite interval (e.g., Case-IV to VI), a significant rectification ratio ($\gamma \geq 3.29$) is maintained. By varying the system size, the rectification ratio γ can increase from 1.95 to 11.06 due to the sharp rise in the forward heat current density. The thermal rectification ratio exhibits a non-monotonic trend, first increasing and then decreasing with system size, indicating an optimal size range for achieving maximum rectification.

This novel thermal diode design, integrating thermal rectification and cloaking effects, enables dual-functional thermal management and thermal camouflage in specific scenarios. It is suitable for applications such as aerospace and microelectronics, which require precise heat flux control and thermal protection, and provides a new strategy for actively controlling the direction and path of heat flow. The non-monotonic dependence of the rectification ratio on system width is explained based on the thermal resistance distribution and heat flow paths, offering physical insights that align with simulation results. Since the present study emphasizes functional integration and tunability within a structural framework, a phenomenological understanding is provided to highlight key behaviors. Future work will aim to establish a more general theoretical framework to further elucidate the coupling between geometric factors and nonlinear thermal transport.

References

[1] Li N B, Ren J, Wang L, Zhang G, Hänggi P and Li B W 2012 *Rev. Mod. Phys.* **84** 1045
[2] Ding Y F, Zhu G M, Shen X Y, Bai X and Li B W 2022 *Chin. Phys. B* **31** 126301
[3] Terraneo M, Peyrard M and Casati G 2002 *Phys. Rev. Lett.* **88** 094302
[4] Li B W, Wang L and Casati G 2004 *Phys. Rev. Lett.* **93** 184301
[5] Li B W, Lan J H and Wang L 2005 *Phys. Rev. Lett.* **95** 104302
[6] Kuo D M T and Chang Y C 2010 *Phys. Rev. B* **81** 205321
[7] Roberts N A and Walker D G 2012 *J. Heat Transfer* **133** 092401
[8] Xie R G, Bui C T, Varghense B, Zhang Q X, Sow C H, Li B W and Thong J T L 2011 *Adv. Funct. Mater.* **21** 1602
[9] Li T, Jiang W T, Zhang Y, Li B T, Wang L L, Niu D, Liu H Z, Yin L, Shi Y S, Chen B D, Chen J J, Liu X K and Peng D L 2022 *Adv. Funct. Mater.* **32** 2111229
[10] Joulain K, Derevillon J, Ezzahri Y and Ordonez-Miranda J 2016 *Phys. Rev. Lett.* **115** 200601
[11] Zhang Y C, Yang Z M, Zhang X, Lin B H, Lin G X and Chen J C 2018 *Europhys. Lett.* **122** 17002
[12] Klinar K, Rojo M M, Kutnjak Z and Kitanovski A 2020 *J. Appl. Phys.* **127** 234101
[13] Lyu J, Sheng Z Z, Xu Y Y, Liu C M and Zhang X T 2022 *Adv. Funct. Mater.* **32** 2200137
[14] Chang C W, Okawa D, Majumdar A and Zettl A 2006 *Science* **314** 1121
[15] Yang N, Zhang G and Li B W 2009 *Appl. Phys. Lett.* **95** 033107
[16] Wang H D, Hu S Q, Takahashi K, Zhang X, Takamatsu H and Chen J 2017 *Nat. Commun.* **8** 15843
[17] Wang J and Zheng Z G 2010 *Phys. Rev. E* **81** 011114
[18] Shrestha R, Luan Y, Luo X, Shin S, Zhang T, Smith P, Gong W, Bockstaller M, Luo T, Chen R, Hippalgaonkar K and Shen S 2020 *Nat. Commun.* **11** 4346
[19] Li H Y, Wang J and Xia G D 2023 *Chin. Phys. B* **32** 054401
[20] Cao B, Han C Z, Hao X, Wang C and Lu J C 2024 *Chin. Phys. Lett.* **41** 077302
[21] Hu B, Yang L and Zhang Y 2006 *Phys. Rev. Lett.* **97** 124302
[22] Peyrard M 2006 *Europhys. Lett.* **76** 49
[23] Hu B, He D, Yang L and Zhang Y 2006 *Phys. Rev. E* **74** 060201
[24] Dames C 2009 *J. Heat Transfer* **131** 061301
[25] Go D B and Sen M 2010 *J. Heat Transfer* **132** 124502
[26] Wang J, Shao C R, Li H Y and Xia G D 2022 *Int. J. Heat Mass Transfer* **188** 122627
[27] Du F Y, Zhang W, Wang H Q and Zheng J C 2023 *Chin. Phys. B* **32** 064402
[28] Li Y, Li J X, Qi M H, Qiu C W and Chen H S 2021 *Phys. Rev. B* **103** 014307
[29] Li Y, Shen X Y, Wu Z H, Huang J Y, Chen Y X, Ni Y S and Huang J P 2015 *Phys. Rev. Lett.* **115** 195503
[30] Li Y, Shen X Y, Huang J P and Ni Y S 2016 *Phys. Lett. A* **380** 1641
[31] Xue M Z, Wang J and Xia G D 2025 *Int. J. Heat Mass Transfer* **240** 126647
[32] Fan C Z, Gao Y and Huang J P 2008 *Appl. Phys. Lett.* **92** 251907
[33] Han T C, Bai X, Gao D L, Thong J T L, Li B W and Qiu C W 2014 *Phys. Rev. Lett.* **112** 054302
[34] Han T C, Bai X, Thong J T L, Li B W and Qiu C W 2014 *Adv. Mater.* **26** 1731
[35] Guenneau S, Amra C and Veynante D 2012 *Opt. Express* **20** 8207
[36] Li Y, Bai X, Yang T Z, Luo H L and Qiu C W 2018 *Nat. Commun.* **9** 273
[37] Zhang J, Zhang H C, Huang Z L, Sun B W and Li Y Y 2022 *Chin. Phys. B* **31** 014402
[38] Sun T, Wang X H, Yang X Y, Meng T, He R Y and Wang Y X 2022 *Int. J. Heat Mass Transfer* **187** 122568
[39] Feng H L, Zhang X W, Zhou L M, Zhang Y K and Ni Y S 2024 *Chin. Phys. B* **33** 038102
[40] Xu H Y, Shi X H, Gao F, Sun H D and Zhang B L 2014 *Phys. Rev. Lett.* **112** 054301
[41] Nguyen D M, Xu H Y, Zhang Y M and Zhang B L 2015 *Appl. Phys. Lett.* **107** 121901

[42] Han T C, Yang P, Li Y, Lei D Y, Li B W, Hippalgaonkar K and Qiu C W 2018 *Adv. Mater.* **30** 1804019
[43] Su C, Xu L J and Huang J P 2020 *Europhys. Lett.* **130** 34001
[44] Shan Q R, Shao C R, Wang J and Xia G D 2023 *Chin. Phys. Lett.* **40** 104401
[45] Xu L J, Jiang C R, Shang J, Wang R Z and Huang J P 2017 *Eur. Phys. J. B* **90** 221
[46] Uyanna O and Najafi H 2020 *Acta Astronaut.* **176** 341
[47] Yang Y, Chen H Y, Wang H, Li N B and Zhang L F 2018 *Phys. Rev. E* **98** 042131
[48] Herrera F A, Luo T F and Go D B 2018 *J. Heat Transfer* **139** 091301
[49] Oh D W, Ko C, Ramanathan S and Cahill D G 2010 *Appl. Phys. Lett.* **96** 151906
[50] Liu L N, Hou Y, Yin X Z, Zhang F and Peng Z F 2018 *Funct. Mater. Lett.* **12** 1950015
[51] Zhang T and Lou T F 2013 *ACS Nano* **7** 7592